Wideband generalized admittance matrix representation for the analysis and design of waveguide filters with coaxial excitation

Fermín Mira,[1] Ángel A. San Blas,[2] Vicente E. Boria,[3] Luis J. Roglá,[4] and Benito Gimeno[5]

[1]   A very efficient technique for the full-wave analysis and design of complex passive waveguide filters, including rectangular cavities with metallic cylindrical posts and coaxial excitation, is presented. This novel technique provides the wideband generalized admittance matrix representation of the whole structure in the form of pole expansions, thus extracting the most expensive computations from the frequency loop. For this purpose, the structure is properly segmented into its key building blocks, all of them characterized in terms of wideband admittance matrices. Then, an efficient iterative algorithm for combining these matrices, and finally providing the wideband generalized admittance matrix of the complete structure, is followed. In order to validate the accuracy and efficiency of this full-wave modal technique, four different waveguide filters have been considered. In particular, the design of a compact four-pole in-line filter with tuning screws and of an evanescent-mode filter, both operating in the X-band and including a standard (vertical) coaxial excitation, are first presented. Finally, two C-band six-resonator comb-line filters, one of them with a cross-coupling configuration, and both excited with a collinear end-launcher transition based on a disc-ended coaxial, are also designed. Numerical data from a commercial software, as well as measurements of a manufactured prototype, are included for verification purposes.

1.   Introduction

[2]   The fast-growing microwave and millimeter-wave equipment market creates a constant demand for faster and more efficient computer-aided design (CAD) tools that must be able to meet the requirements of a computationally inexpensive design process. Moreover, modern high-capacity telecommunication equipment is based on a wide variety of waveguide components, which are usually fed using a coaxial excitation [*Uher et al.*, 1993]. For instance, standard coaxial cavity filters (either with in-line or folded configurations) and recently proposed orthogonal coaxial filters, all of them typically operating at low-frequency bands (i.e., L-, S- and C-bands), are commonly excited using a collinear end-launcher transition from a coaxial to a rectangular waveguide [*Morini*

et al., 2006, 2007; *Höft and Yousif*, 2011]. Evanescent-mode filters, in-line filters, and thick-iris waveguide filters [*Liang et al.*, 1992] are also classically fed using a standard (vertical) coaxial excitation. Besides, as it will be discussed afterward, the integration of the coaxial excitation in the input and output waveguides of the structure can be used to raise the order of the designed filter (and then to enhance the response selectivity) without increasing its length. As a consequence, the coaxial-line to rectangular waveguide transition can be considered as a basic building block of a wide variety of microwave and millimeter-wave components, and its integration in general CAD tools becomes crucial to ensure a rigorous and efficient design of all these passive components.

[3]   In addition, most of the aforementioned types of filters usually include rectangular waveguide sections with partial-height metallic posts, and this key building block is also found in many other waveguide devices, such as adapters, mode-launchers, comb-line, and interdigital filters [*Ihmels and Arndt*, 1993; *Levy et al.*, 1997]. Furthermore, this basic building block also allows to model real tuning screws, which are widely employed in practical implementations of dual-mode and direct-coupled rectangular waveguide filters [*Chang and Zaki*, 1991; *Boria et al.*, 1998]. The usual presence of these practical filters in most of present communication systems (e.g., mobile and satellite ones) demands the availability of fast CAD tools, while preserving a high degree of accuracy.

[4]   Several attempts to achieve the required efficient and accurate CAD tools have been already performed.

[1]Centre Tecnològic de Telecomunicacions de Catalunya, Barcelona, Spain.
[2]Departamento de Ingeniería de Comunicaciones, Universidad Miguel Hernández de Elche, Elche, Spain.
[3]Departamento de Comunicaciones, Universidad Politécnica de Valencia, Valencia, Spain.
[4]Thales Alenia Space España, Madrid, Spain.
[5]Departamento de Física Aplicada y Electromagnetismo, Valencia, Spain.

Corresponding author: A. A. San Blas, Departamento de Ingeniería de Comunicaciones, Universidad Miguel Hernández de Elche, Avenida de la Universidad s/n, 03202 Elche (Alicante), Spain. (aasanblas@umh.es)

For instance, strictly numerical or mode-matching methods, as well as the combination of both approaches in hybrid solutions, have been tried [*Yao et al.*, 1995; *Gentili*, 2001]. Although these techniques provide enough accurate results, they cannot be optimal for CAD purposes because of their required computing time. A very fast S-domain method for the accurate modeling of rectangular cavities with several conducting posts (arbitrarily placed and oriented) was proposed by *Mira et al.* [2005a]. Then, a very preliminary contribution for the analysis of standard (vertical) coaxial to rectangular waveguide transitions was presented in reference *San Blas et al.* [2006]. These works, based on the well-known 3D boundary integral-resonant mode expansion (BI-RME) method [*Arcioni et al.*, 2002], provide a *Y*-matrix given in the form of pole expansions in the frequency domain for the accurate characterization of such two basic blocks.

[5] The numerical efficiency of these full-wave modal analysis techniques has been greatly improved by means of the so-called segmentation technique [*Mansour and MacPhie*, 1986; *Alessandri et al.*, 1988, 1992; *Guglielmi*, 1994], which consists on decomposing the analysis of a complete waveguide structure into the characterization of its elementary key building blocks. The work proposed in reference *Mira et al.*, 2005b makes use of this segmentation technique by combining the analysis of resonant cavities using the BI-RME method [*Mira et al.*, 2005a] with the integral equation technique for characterizing planar waveguide junctions [*Gerini et al.*, 1998]. However, in the above-mentioned work (i.e., *Mira et al.* [2005b]), the analysis of the planar junctions and the cascade connection of the different wideband matrices must be performed at each frequency point, thus dramatically increasing the computational cost of the design process.

[6] In this paper, the main objective consists of developing a very efficient CAD tool, which must be able to avoid the repetition of the cumbersome computations performed in the frequency domain, for the analysis and design of complex waveguide devices composed of rectangular cavities loaded with partial-height metallic cylindrical posts, planar waveguide junctions, uniform waveguide sections, and boxed resonators including a coaxial excitation (either vertical or collinear). To this aim, the 3D BI-RME method is first applied

to derive a wideband *Y*-matrix used to characterize boxed resonators with inserted metallic posts that can be fed by a generalized coaxial probe. Next, the new formulation proposed in reference *Mira et al.* [2008] is used to characterize the planar waveguide junctions of the structure, thus obtaining a *Y*-matrix with the same form as the one provided by the BI-RME formulation. Finally, the algorithm proposed in reference *Arcioni and Conciauro* [1999], which has been extended to cope with folded structures including cross-couplings, allows the wideband cascade connection of the previous key building blocks preserving the same form of the pole expansions for the *Y*-matrices. As a result, all the main computations are performed out of the frequency loop, thus reducing the computational effort of the new developed CAD tool. In addition, the *Y*-matrix in the form of pole expansions is preserved for the whole structure, allowing for a circuital representation of the device [*Bozzi et al.*, 2009], that can be very useful for synthesis and design purposes. This CAD tool has been successfully used to design four different waveguide filters, all of them including integrated coaxial excitations and partial-height conducting posts: a compact four-pole in-line filter with tuning screws, an evanescent-mode filter with cylindrical posts, and two C-band comb-line filters, one of them with a cross-coupling configuration.

2. Theoretical Description of Basic Blocks

[7] The structure under analysis is first segmented into its basic building blocks. For instance, Figure 1 shows a waveguide structure that includes all these key building blocks, that is, a boxed resonator with a conducting post and an integrated coaxial excitation, different coupling windows, uniform waveguide sections, and a resonant cavity loaded with a partial-height metallic post. Our aim is to represent each basic building block of such equivalent circuit in terms of a wideband generalized admittance matrix (or *Y*-matrix) in the form of pole expansions:

$$\mathbf{Y} = \frac{1}{j\eta k}\mathbf{A} + \frac{jk}{\eta}\mathbf{B} + \frac{jk^3}{\eta}\mathbf{C}\left(\Delta^2 - k^2\mathbf{U}\right)^{-1}\mathbf{C}^T \qquad (1)$$

where $k = \omega\sqrt{\mu\varepsilon}$; $\eta = \sqrt{\mu/\varepsilon}$; and $\mathbf{A}$, $\mathbf{B}$, $\mathbf{C}$, Δ, and $\mathbf{U}$ are frequency-independent matrices. Specifically, $\mathbf{A}$ and $\mathbf{B}$ are
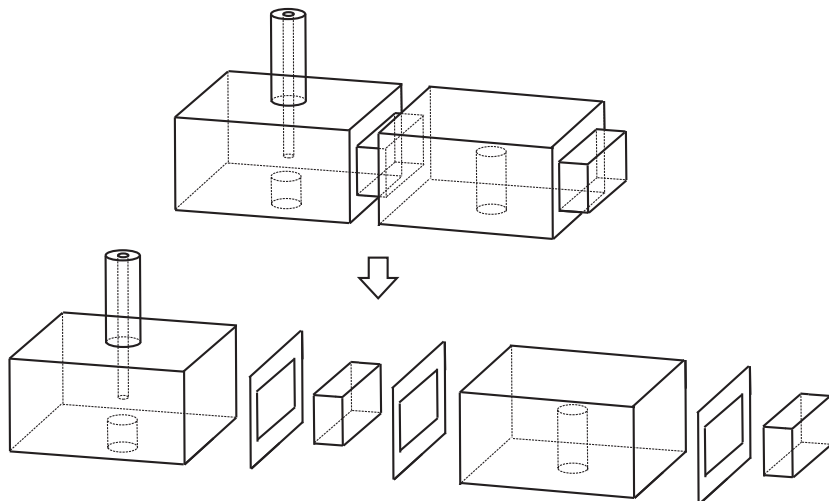
Figure 1. Segmentation strategy for the structure under study.

square symmetric matrices of size N (N being the total number of accessible modes considered in each waveguide section); **C** is a matrix of size $N \times Q$, Q being the number of terms included in the pole expansion; Δ is a diagonal matrix containing the values of the considered poles; and **U** is the unitary matrix of size Q.

[8] According to Figure 1, we will compute the wideband admittance matrices in the form of (1) for the boxed resonator fed by the coaxial probe, the planar junctions, the uniform waveguide sections, and the resonant cavities including conducting posts. Next, we will derive the expressions for computing the elements of all such matrices.

2.1. Planar Waveguide Steps

[9] First, we consider the planar junction between two arbitrary waveguides shown in Figure 2. Following the integral equation technique described in reference *Gerini et al.* [1998], such junction can be represented in terms of a generalized *Y*-matrix (**Y**$_{st}$), and two sets of asymptotic modal impedances (see Figure 2), which represent the impedances related to higher-order modes and are determined as follows:

$$\hat{Z}_m^{(\delta)} = \lim_{m \to \infty} Z_m^{(\delta)} = \begin{cases} jk\eta / \kappa_m^{(\delta)} & \text{TE modes} \\ \kappa_m^{(\delta)} \eta / (jk) & \text{TM modes} \end{cases} \quad (2)$$

where $Z_m^{(\delta)}$ and $\kappa_m^{(\delta)}$ represent, respectively, the modal impedance and the cutoff wave number of the mth mode at waveguide port δ ($\delta = 1, 2$), whose definitions for standard TE and TM modes can be found in reference *Marcuvitz, 1986*. Note that these asymptotic impedances will be also represented as independent networks in the form of a *Y*-matrix, as it is described in the next subsection.

[10] In order to yield the expressions for the elements of the generalized *Y*-matrix of the planar junction (**Y**$_{st}$ in Figure 2), an integral equation is first set up for the magnetic field at the junction plane [*Gerini et al.*, 1998]. Next, the procedure proposed in reference *Mira et al.* [2008] is followed, and the method of moments is then used to obtain a linear system, whose solution is finally found by solving an eigenvalue problem to avoid the inversion of matrices for each frequency point. As a result, the set of frequency-independent matrices present in (1) is computed, and the desired expression in the form of pole expansions for the generalized matrix **Y**$_{st}$ is finally derived (see more details in reference *Mira et al.* [2008]).

2.2. Asymptotic Impedances

[11] Each set of asymptotic modal impedances presented in (2) can be seen as a two-port network, which can be easily

characterized by a generalized *Y*-matrix whose elements are defined as follows:

$$Y_{m,n}^{(\delta,\gamma)} = -\frac{\delta_{m,n}}{\hat{Z}_m} = \delta_{m,n} \begin{cases} -\dfrac{\kappa_m^{(\delta)}}{jk\eta} & \text{TE} \\ -\dfrac{jk}{\kappa_m^{(\delta)}\eta} & \text{TM} \end{cases} \quad (3)$$

where $\delta_{m,n}$ stands for the well-known Kronecker's delta (i.e., $\delta_{m,n} = 1$ if $m = n$, and $\delta_{m,n} = 0$ otherwise). The previous expression is suitable for the representation of the generalized admittance matrix as indicated by (1). In this case, the pole expansion is not present and, therefore, we can obtain the following frequency-independent matrices:

$$A_{m,n}^{(\delta,\gamma)} = \delta_{m,n} \begin{cases} -\kappa_m^{(\delta)} & \text{TE} \\ 0 & \text{TM} \end{cases} \quad (4)$$

$$B_{m,n}^{(\delta,\gamma)} = \delta_{m,n} \begin{cases} 0 & \text{TE} \\ -1/\kappa_m^{(\delta)} & \text{TM} \end{cases} \quad (5)$$

[12] After considering the asymptotic impedances of the waveguide steps, the uniform waveguide sections that interconnect them must be solved. The expressions for the generalized admittance matrix of a section of a uniform waveguide of length l can be found in reference *Arcioni and Conciauro* [1999].

2.3. Rectangular Cavities with Conducting Posts

[13] This key building block consists of a section of rectangular waveguide containing multiple conducting posts of cylindrical shape. The analysis of this basic block has been performed following the method described in reference *Mira et al.* [2005a]. This method, based on the BI-RME technique [*Arcioni et al.*, 2002], has been particularized for the proposed structure to optimize the computation by reducing the number of unknowns, and by solving analytically an important part of the involved integrals, thus resulting in very reduced order models that are of great utility for our CAD tool. The key point of this approach is the inclusion in the algorithm of optimized Green's functions for rectangular domains [*Bressan et al.*, 2000], which allows to perform numerical integrations over the surface of the conducting posts only, the use of special basis functions for cylindrical surfaces, and the analytical solution of the integrals over the waveguide access ports.

[14] The resulting *Y*-matrix has the form indicated in (1), and the frequency-independent matrices **A**, **B**, and **C** include the following terms:
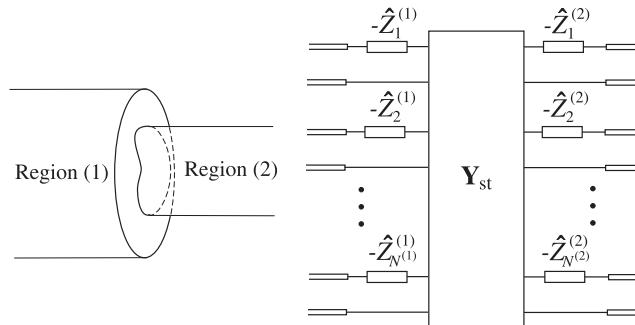
Figure 2. Equivalent circuit representation of the planar waveguide junction.

$$\mathbf{M}_1^{rp} = \int_S \int_S \mathbf{F}_r(\mathbf{r}) \cdot \mathbf{G}(\mathbf{r}, \mathbf{r}') \cdot \mathbf{F}_p(\mathbf{r}') dS dS' \tag{6}$$

$$\mathbf{M}_2^{rp} = \int_S \int_S \nabla_S \cdot \mathbf{F}_r(\mathbf{r}) g(\mathbf{r}, \mathbf{r}') \nabla_S' \cdot \mathbf{F}_p(\mathbf{r}') dS dS' \tag{7}$$

$$\mathbf{M}_3^{mp} = \int_S \mathbf{E}_m(\mathbf{r}) \cdot \mathbf{F}_p(\mathbf{r}) dS \tag{8}$$

$$\mathbf{M}_4^{mp} = \int_S \mathbf{e}_m(\mathbf{r}) \cdot \mathbf{F}_p(\mathbf{r}) p(\mathbf{r}) dS \tag{9}$$

where $\mathbf{F}$ represents the set of chosen basis functions to model the current over the metallic post, $\mathbf{G}$ and g are the dyadic and scalar Green's functions of a standard rectangular (boxed) resonator where the singularity has been previously extracted, $\mathbf{E}_m$ is the electric field related to the mth resonant mode of the rectangular cavity, $\mathbf{e}_m$ is the mth normalized electric-type vector mode function over the waveguide access ports, and $p(\mathbf{r})$ is the resulting function after performing the partial analytical solution of the numerical integrals involving basis functions over the conducting posts and the electromagnetic fields over the waveguide access ports. It is important to mention that all the integrals are performed only over the post surfaces (S). In addition, an eigenvalue problem has to be solved to obtain the corresponding eigenvalues included in the pole expansion, and the related eigenvectors included in matrix $\mathbf{C}$. These eigenvalues represent the wave numbers of the resonant modes of the cavity loaded with the post. The size of this eigenvalue problem depends on the number of basis functions, and on the resonant modes considered for the cavity. Typically, a few hundred of resonant modes and basis functions are enough to obtain a good accuracy.

2.4. Generalized Y-Matrix of a Boxed Resonator with an Integrated Coaxial Excitation

[15] The full-wave analysis of a rectangular cavity fed by a coaxial probe is also performed following the 3D BI-RME method. This technique is used to derive a wideband generalized admittance matrix of a boxed resonator with up to five rectangular waveguide ports and a coaxial access port. To this aim, the authors have extended the theoretical work developed in reference *San Blas et al.* [2006], thus allowing to consider an increased number of access ports. In particular, this novel theoretical extension allows placing the coaxial waveguide port in any face of the considered boxed resonator, while preserving the possibility of adding a rectangular waveguide access port of arbitrary dimensions on each of the remaining resonator sides. Thanks to the flexibility of the implemented CAD tool, the characterization of this key building block permits considering not only a standard coaxial excitation configuration, but also a collinear end-launcher transition from a coaxial line to the rectangular waveguide, which is extensively used for feeding a wide variety of practical microwave and millimeter-wave filters. Furthermore, generalized coaxial probes such as a disc-ended probe are also allowed. A representative example of the described basic building block has been depicted in Figure 3. However, if the coaxial probe was physically contacting the first resonator, a more elaborated algorithm based on a set of more general Rao-Wilton-Glisson basis functions, as described in reference *Quesada et al.* [2010], should be used to compute the Y-matrix of this block.
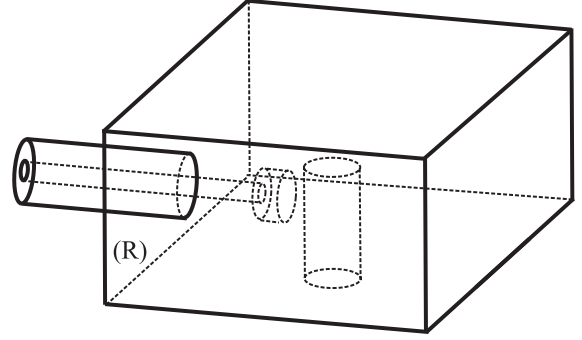
Figure 3. Boxed resonator with an integrated coaxial excitation. The cavity is loaded with a partial-height metallic post, including a collinear end-launcher transition from a disc-ended coaxial line to the rectangular waveguide.

[16] In order to derive the Y-matrix of the structure in the form of (1), the modal chart of the coaxial waveguide needs to be first calculated. To this aim, the radial variation of higher-order modes are expressed using sinusoidal functions [*Gimeno and Guglielmi*, 1997], thus avoiding the more cumbersome Bessel functions. Next, we remind that the elements of the 3D BI-RME matrices $\mathbf{G}_{ij}$ and $\mathbf{T}_{ij}$ needed to characterize the device, and which are included in the matrices $\mathbf{A}$ and $\mathbf{B}$ of expression (1) (see reference *Arcioni et al.* [2002] for more details on these matrices), are singular when the modes i and j are referred to the same waveguide port (the origin of this singularity lies on the divergent behavior of the scalar and dyadic Green's functions). Although this singularity is easily removed when the involved modes belong to a rectangular waveguide access port [*Mira et al.*, 2005a] (this is the case of the previous section), its analytical treatment can be really difficult when the modes are referred to the coaxial waveguide port.

[17] To overcome this problem, the proposed strategy consists of expanding the vector mode functions of the coaxial waveguide in terms of the vector mode functions of the rectangular cavity port fed by the coaxial probe as follows (this auxiliary rectangular waveguide has been marked with the symbol "(R)" in the structure shown in Figure 3):

$$\mathbf{h}^{\mathrm{TEM}}(\mathbf{r}) = \sum_{i=1}^{Q^{\mathrm{TM}}} \upsilon_i^{(\mathrm{TEM})} \mathbf{h}_i^{\mathrm{TM(R)}}(\mathbf{r}) \tag{10}$$

$$\mathbf{h}_m^{\mathrm{TE}}(\mathbf{r}) = \sum_{i=1}^{Q^{\mathrm{TE}}} \sigma_i^{(m)} \mathbf{h}_i^{\mathrm{TE(R)}}(\mathbf{r}) + \sum_{j=1}^{Q^{\mathrm{TM}}} \tau_j^{(m)} \mathbf{h}_j^{\mathrm{TM(R)}}(\mathbf{r}) \tag{11}$$

$$\mathbf{h}_m^{\mathrm{TM}}(\mathbf{r}) = \sum_{i=1}^{Q^{\mathrm{TM}}} v_i^{(m)} \mathbf{h}_i^{\mathrm{TM(R)}}(\mathbf{r}) \tag{12}$$

[18] In these expressions, Q^{TE} and Q^{TM} represent, respectively, the number of TE and TM modes of the expansion considered in the rectangular waveguide fed by the coaxial probe; $\mathbf{h}_i^{\mathrm{TE(R)}}(\mathbf{r})$ and $\mathbf{h}_i^{\mathrm{TM(R)}}(\mathbf{r})$ are the TE and TM normalized magnetic-type vector mode functions related to the corresponding ith mode of this auxiliary rectangular waveguide; and $\upsilon_i^{(\mathrm{TEM})}$, $\sigma_i^{(m)}$, $\tau_i^{(m)}$, and $v_i^{(m)}$ represent the corresponding coupling coefficient between the mth mode of the coaxial waveguide port (for $m = 1$ we have the TEM mode) and the ith mode of the

rectangular waveguide fed by the coaxial probe. The coupling coefficients are readily calculated as:

$$v_i^{(\text{TEM})} = \int_S \mathbf{h}^{(\text{TEM})}(\mathbf{r}) \cdot \mathbf{h}_i^{\text{TM(R)}}(\mathbf{r}) dS \tag{13}$$

$$\sigma_i^{(m)} = \int_S \mathbf{h}_m^{\text{TE}}(\mathbf{r}) \cdot \mathbf{h}_i^{\text{TE(R)}}(\mathbf{r}) dS \tag{14}$$

$$\tau_i^{(m)} = \int_S \mathbf{h}_m^{\text{TE}}(\mathbf{r}) \cdot \mathbf{h}_i^{\text{TM(R)}}(\mathbf{r}) dS \tag{15}$$

$$v_i^{(m)} = \int_S \mathbf{h}_m^{\text{TM}}(\mathbf{r}) \cdot \mathbf{h}_i^{\text{TM(R)}}(\mathbf{r}) dS \tag{16}$$

[19] Once the vector mode functions of the coaxial access port have been expanded in this way, the singularity of the 3D BI-RME matrices can be easily removed as in the case of the standard rectangular waveguide access ports, and the Y-matrix in the form of (1) for the resonator including the coaxial excitation can be readily derived following the 3D BI-RME method.

3. Cascade Connection of the Y-Matrices

[20] Once the expressions for the Y-matrices of all the elementary blocks of the structure shown in Figure 1 have been derived, we make use of the efficient algorithm proposed in reference *Arcioni and Conciauro* [1999] for cascading Y-matrices in the form of pole expansions. In this section, we only show the particular case of a cross-coupling configuration (which is not included in reference *Arcioni and Conciauro* [1999]), where internal ports must also be connected. In addition, we propose a very efficient iterative algorithm for characterizing devices composed of a large number of cascaded planar waveguide junctions.

3.1. Internal Port Connection of Y-Matrices in the Form of Pole Expansions

[21] Let us consider the four-resonator folded comb-line filter configuration shown in Figure 4 (note the cross-coupling between the input and the output resonators), whose generalized Y-matrices are given in the form of pole expansions. The algorithm proposed in reference *Arcioni and Conciauro* [1999] can be applied for the consecutive connection of

cavities 1–2–3–4, where it is assumed that two building blocks with external and internal ports are interconnected at each stage. However, this is not the case for the example of Figure 4, where after performing the consecutive cascade connection of the four cavities, the resulting structure is a single block where the two sets of internal ports to be connected belong to the same block.

[22] For solving this particular case, we follow the network representation depicted in the right side of Figure 4. The currents and voltages at the external ports are grouped into the vectors $\mathbf{i}_e$ and $\mathbf{v}_e$, whereas the currents and voltages at the interconnected ports are collected into the vectors $\mathbf{i}_c^{(1)}$, $\mathbf{i}_c^{(2)}$, $\mathbf{v}_c^{(1)}$ and $\mathbf{v}_c^{(2)}$. If we consider that the currents are incoming to the circuit we can write:

$$\mathbf{i}_c^{(1)} = \mathbf{Y}_{cc}^{(1,1)}\mathbf{v}_c^{(1)} + \mathbf{Y}_{ce}^{(1)}\mathbf{v}_e + \mathbf{Y}_{cc}^{(1,2)}\mathbf{v}_c^{(2)} \tag{17}$$

$$\mathbf{i}_c^{(2)} = \mathbf{Y}_{cc}^{(2,1)}\mathbf{v}_c^{(1)} + \mathbf{Y}_{ce}^{(2)}\mathbf{v}_e + \mathbf{Y}_{cc}^{(2,2)}\mathbf{v}_c^{(2)} \tag{18}$$

where the matrices on the right-hand side are obtained by a suitable arrangement of the entries of matrix $\mathbf{Y}$. Then, after enforcing the continuity of the currents and voltages at the interconnected ports ($\mathbf{v}_c = \mathbf{v}_c^{(1)} = \mathbf{v}_c^{(2)}$ and $\mathbf{i}_c^{(1)} = -\mathbf{i}_c^{(2)}$), we obtain the following expression:

$$\left(\mathbf{Y}_{cc}^{(1,1)} + \mathbf{Y}_{cc}^{(1,2)} + \mathbf{Y}_{cc}^{(2,1)} + \mathbf{Y}_{cc}^{(2,2)}\right)\mathbf{v}_c = -\left(\mathbf{Y}_{ce}^{(1)} + \mathbf{Y}_{ce}^{(2)}\right)\mathbf{v}_e \tag{19}$$

[23] The current at the external ports can be expressed as follows:

$$\mathbf{i}_e = \mathbf{Y}_{ee}\mathbf{v}_e + \left(\mathbf{Y}_{ec}^{(1)} + \mathbf{Y}_{ec}^{(2)}\right)\mathbf{v}_c \tag{20}$$

[24] We can easily arrange the previous set of equations (19) and (20) into a linear system in matrix form:

$$\mathbf{i}_e = \mathbf{Y}_e\mathbf{v}_e + \mathbf{Y}_s\mathbf{v}_c \tag{21}$$

$$\mathbf{Y}_c\mathbf{v}_c = -\mathbf{Y}_s\mathbf{v}_e \tag{22}$$

where the matrices $\mathbf{Y}_e$, $\mathbf{Y}_s$, and $\mathbf{Y}_c$ are given by:

$$\mathbf{Y}_e = \mathbf{Y}_{ee} \tag{23}$$

$$\mathbf{Y}_s = \mathbf{Y}_{ec}^{(1)} + \mathbf{Y}_{ec}^{(2)} \tag{24}$$
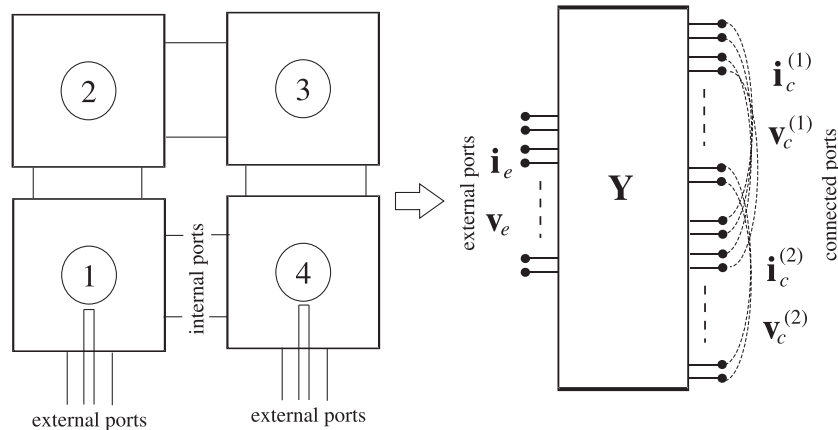
Figure 4. Example of a filter with cross-coupling and its network representation.

$$\mathbf{Y}_c = \mathbf{Y}_{cc}^{(1,1)} + \mathbf{Y}_{cc}^{(1,2)} + \mathbf{Y}_{cc}^{(2,1)} + \mathbf{Y}_{cc}^{(2,2)} \qquad (25)$$

[25] Our final goal is to obtain the overall matrix $\mathbf{Y}_{tot}$, relating the vectors $\mathbf{i}_e$ and $\mathbf{v}_e$, in the form of (1). Proceeding in this way, we will avoid repeating matrix multiplications and inversions frequency by frequency. For such purposes, we first express the matrices $\mathbf{Y}_e$, $\mathbf{Y}_s$, and $\mathbf{Y}_c$ in the form of pole expansions. Taking into account the definitions of the matrices included in Table 1, we can easily write that:

$$\mathbf{Y}_e = \frac{1}{jk\eta}\mathbf{A}_e + \frac{jk}{\eta}\mathbf{B}_e + \frac{jk^3}{\eta}\mathbf{C}_e\left(\Delta^2 - k^2\mathbf{U}\right)^{-1}\mathbf{C}_e^T \qquad (26)$$

$$\mathbf{Y}_s = \frac{1}{jk\eta}\mathbf{A}_s + \frac{jk}{\eta}\mathbf{B}_s + \frac{jk^3}{\eta}\mathbf{C}_e\left(\Delta^2 - k^2\mathbf{U}\right)^{-1}\mathbf{C}_c^T \qquad (27)$$

$$\mathbf{Y}_c = \frac{1}{jk\eta}\mathbf{A}_c + \frac{jk}{\eta}\mathbf{B}_c + \frac{jk^3}{\eta}\mathbf{C}_c\left(\Delta^2 - k^2\mathbf{U}\right)^{-1}\mathbf{C}_c^T \qquad (28)$$

[26] At this point, the algorithm in reference *Arcioni and Conciauro* [1999] is followed, where the partitioning of $\mathbf{A}_c$, $\mathbf{B}_c$, $\mathbf{C}_c$, $\mathbf{A}_s$, and $\mathbf{B}_s$ matrices in terms of submatrices involving the TE modes (submatrices with the superscript ') and the TM modes (submatrices with the superscript ") is performed as indicated in Table 2. Moreover, according to appendix A of *Arcioni and Conciauro* [1999], note that matrices $\mathbf{A}_c$ and $\mathbf{A}_s$ are equal to 0 for indexes where TM modes are involved. Then, an eigenvalue problem has to be solved to derive the overall matrix $\mathbf{Y}_{tot}$ in the desired form. Once the internal ports have been connected, a new expression for the Y-matrix is obtained from (1) considering:

$$\mathbf{A}_{tot} = \mathbf{A}_e - \mathbf{A}_s'\mathbf{A}_c'^{-1}\mathbf{A}_s'^T \qquad (29)$$

$$\mathbf{B}_{tot} = \mathbf{E} + \mathbf{A}_s'\mathbf{V}\mathbf{K}^{-4}\mathbf{V}^T\mathbf{A}_s'^T - \mathbf{A}_s'\mathbf{A}_c'^{-1}\mathbf{F}^T - \mathbf{F}\mathbf{A}_c'^{-1}\mathbf{A}_s'^T \qquad (30)$$

$$\mathbf{C}_{tot} = \mathbf{F}\mathbf{V} + \mathbf{G}\mathbf{W} - \mathbf{A}_s'\mathbf{V}\mathbf{K}^{-2} \qquad (31)$$

where we have:

$$\mathbf{E} = \mathbf{B}_e - \mathbf{B}_s''\mathbf{B}_c''^{-1}\mathbf{B}_s''^T \qquad (32)$$

$$\mathbf{F} = \mathbf{B}_s' - \mathbf{B}_s''\mathbf{B}_c''^{-1}\mathbf{B}_m^T \qquad (33)$$

$$\mathbf{G} = \mathbf{C}_e - \mathbf{B}_s''\mathbf{B}_c''^{-1}\mathbf{C}_c'' \qquad (34)$$

and $\mathbf{K}$, $\mathbf{V}$, and $\mathbf{W}$ are matrices related with the eigensolutions of the problem. In particular, $\mathbf{K}$ is a diagonal matrix containing

Table 1. Definition of matrices

$\mathbf{A}_c = \left[\mathbf{A}_{cc}^{(1,1)} + \mathbf{A}_{cc}^{(1,2)} + \mathbf{A}_{cc}^{(2,1)} + \mathbf{A}_{cc}^{(2,2)}\right]$
$\mathbf{B}_c = \left[\mathbf{B}_{cc}^{(1,1)} + \mathbf{B}_{cc}^{(1,2)} + \mathbf{B}_{cc}^{(2,1)} + \mathbf{B}_{cc}^{(2,2)}\right]$
$\mathbf{C}_c = \left[\mathbf{C}_c^{(1)} + \mathbf{C}_c^{(2)}\right]\,\mathbf{A}_s = \left[\mathbf{A}_{ec}^{(1)} + \mathbf{A}_{ec}^{(2)}\right]\,\mathbf{B}_s = \left[\mathbf{B}_{ec}^{(1)} + \mathbf{B}_{ec}^{(2)}\right]$

Table 2. Partitioning of matrices

$\mathbf{A}_c = \begin{bmatrix} \mathbf{A}_c' & 0 \\ 0 & 0 \end{bmatrix} \quad \mathbf{B}_c = \begin{bmatrix} \mathbf{B}_c' & \mathbf{B}_m \\ \mathbf{B}_m^T & \mathbf{B}_c'' \end{bmatrix} \quad \mathbf{C}_c = \begin{bmatrix} \mathbf{C}_c' \\ \mathbf{C}_c'' \end{bmatrix}$
$\mathbf{A}_s = \begin{bmatrix} \mathbf{A}_s' 0 \end{bmatrix} \quad \mathbf{B}_s = \begin{bmatrix} \mathbf{B}_s' \mathbf{B}_s'' \end{bmatrix}$

the eigenvalues, whereas $\mathbf{V}$ and $\mathbf{W}$ contain the corresponding eigenvectors.

3.2. Efficient Cascade Connection for Large Structures

[27] When two building blocks of a structure are cascaded, the number of terms in the resulting pole expansion is equal to the number of poles of each block plus the number of TE accessible modes at the common port. If the structure is composed of a large number of blocks, the overall number of poles will become very high, thus reducing the efficiency of the algorithm due to the size of the successive eigenvalue problems.

[28] For avoiding such drawback, we propose to limit the number of eigenvalues considered after each connection. The proposed method was successfully applied in reference *Mira et al.* [2009] for the case of Z-matrices. When two different blocks are connected, we obtain the entries of the generalized Y-matrix in the following form:

$$Y_{m,n}^{(\delta,\gamma)} = \frac{1}{jk\eta}A_{m,n}^{(\delta,\gamma)} + \frac{jk}{\eta}B_{m,n}^{(\delta,\gamma)} + \frac{jk^3}{\eta}\sum_{i=1}^{Q}\frac{C_{m,i}^{(\delta)}C_{n,i}^{(\gamma)}}{k_i^2 - k^2} \qquad (35)$$

[29] In this equation, the higher terms of the sum have a lower contribution to the final result. Due to this fact, we can only consider Q' eigenvalues in the sum and approximate the contribution of the remaining $Q - Q'$ eigenvalues by:

$$\frac{jk^3}{\eta}\sum_{i=Q'+1}^{Q}\frac{C_{m,i}^{(\delta)}C_{n,i}^{(\gamma)}}{k_i^2 - k^2} \approx \frac{jkk_0^2}{\eta}\sum_{i=Q'+1}^{Q}\frac{C_{m,i}^{(\delta)}C_{n,i}^{(\gamma)}}{k_i^2 - k_0^2} \qquad (36)$$

where k_0 corresponds to the value of k at the center point of the frequency band. Proceeding in such a way, the eigenvalues with lower weight are included within the linear term:

$$Y_{m,n}^{(\delta,\gamma)} \approx \frac{1}{jk\eta}A_{m,n}^{(\delta,\gamma)} + \frac{jk}{\eta}\left(B_{m,n}^{(\delta,\gamma)} + k_0^2\sum_{i=Q'+1}^{Q}\frac{C_{m,i}^{(\delta)}C_{n,i}^{(\gamma)}}{k_i^2 - k_0^2}\right)$$
$$+ \frac{jk^3}{\eta}\sum_{i=1}^{Q'}\frac{C_{m,i}^{(\delta)}C_{n,i}^{(\gamma)}}{k_i^2 - k^2} \qquad (37)$$

thus obtaining a reduced size for the eigenvalue problem to be solved during the next connection, whereas a good accuracy is still preserved. This technique can also be applied to reduce the number of poles involved in the Y-matrix characterization of each single building block.

4. Validation Results

[30] In order to test the accuracy and efficiency of the proposed method, the new CAD tool has been applied to the design of four different filters in waveguide technology: a compact four-pole in-line filter with tuning screws, a five-pole evanescent-mode filter, and two six-resonator folded comb-line filters, one of them with a cross-coupling configuration. It is important to note that all the proposed filters include an integrated coaxial excitation, either standard (vertical) or collinear.

[31] The analysis of the designed filters is performed as follows. First, the basic building blocks of each filter are individually analyzed to derive their respective wideband Y-matrix representations. Next, the cascade connection of the obtained intermediate Y-matrices is performed. To this aim, we start from the building block including the
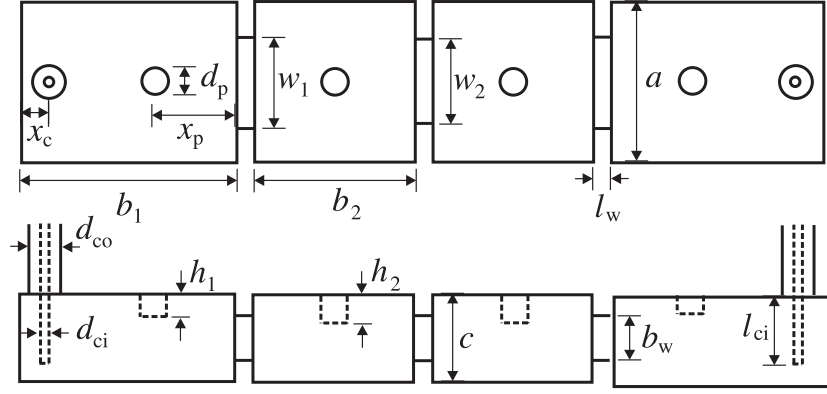
Figure 5. Design of a compact in-line filter with tuning screws, whose dimensions (all in millimeters) are: $d_{ci}=1.0$, $d_{co}=3.5$, $l_{ci}=7.8$, $x_c=3.0$, $x_p=9.0$, $b_1=24.0$, $a=b_2=18.0$, $c=9.525$, $l_w=2.0$, $w_1=10.07$, $w_2=9.3$, $b_w=5.0$, $d_p=3.0$, $h_1=2.45$, $h_2=2.976$.
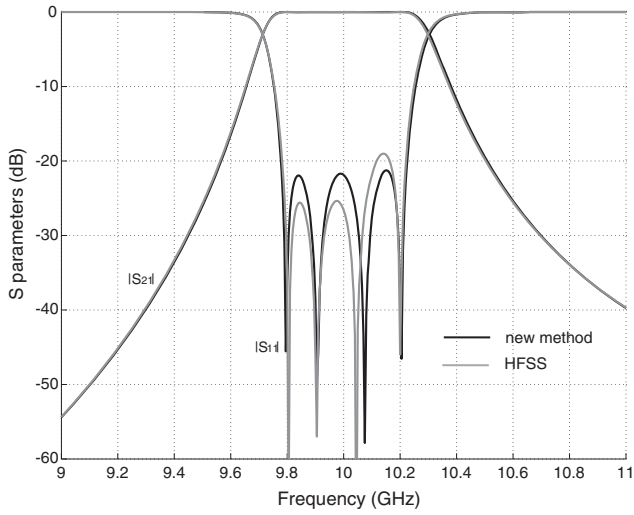
Figure 6. Scattering parameters of the compact in-line filter with tuning screws of Figure 5.

integrated coaxial excitation, and the next building blocks are progressively attached. In the case of symmetrical structures, the building blocks may be added up to the center of the filter and, afterward, we proceed with the cascade connection of the Y-matrices of the two component halves. In the particular case of filters with a cross-coupling configuration, the connection of the internal ports is applied once all the key building blocks have been previously cascaded. This part could be avoided in the case of symmetrical filters when the two halves are cascaded. It is important to mention that the developed CAD tool is general and can therefore deal with completely asymmetrical structures. The cascade connection has been carried out using 30 accessible modes in all the designed filters, and a maximum number of resonant modes for each cavity equal to 250 have been chosen.

[32] The first proposed example consists of a four-pole in-line filter with inserted tuning screws (see Figure 5). It is important to note that the integration of the coaxial line and the insertion of the conducting posts in the input and output waveguides of the device are used to raise the order of the designed in-line filter without increasing its length.
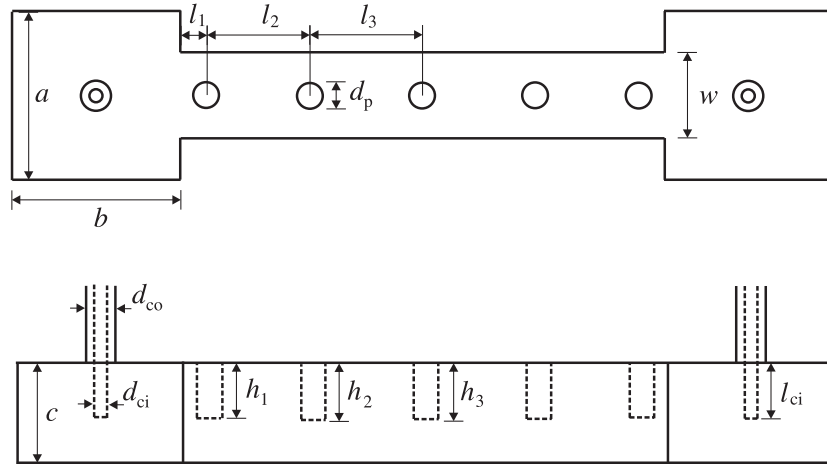
Figure 7. Design of an evanescent-mode filter, whose dimensions (all in millimeters) are: $d_{ci}=1.3$, $d_{co}=3.0$, $l_{ci}=5.5$, $a=b=17.0$, $c=10.16$, $l_1=2.61$, $l_2=10.44$, $l_3=11.455$, $w=8.8$, $d_p=2.5$, $h_1=5.492$, $h_2=5.594$, $h_3=5.59$.

In fact, the input and output sections of the filter have been properly designed to behave as resonators to provide the structure with two additional poles, thus resulting in a more compact filter with enhanced response selectivity.

[33] The filter is fed using a coaxial probe whose impedance is 50 Ω with a relative dielectric permittivity of 2.2. The caption in Figure 5 shows all the physical dimensions
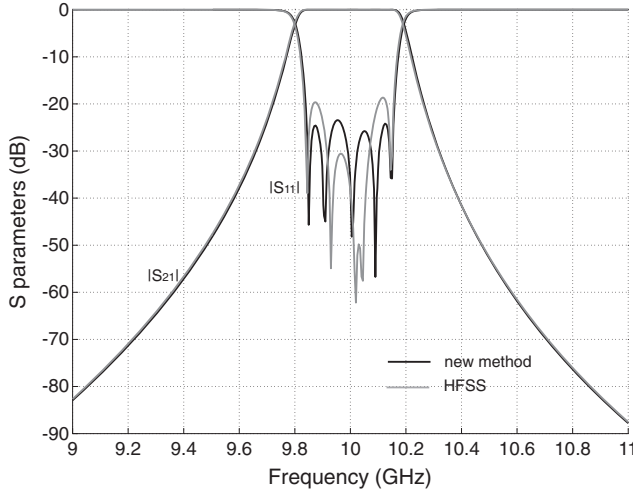
Figure 8. Scattering parameters of the evanescent-mode filter of Figure 7.

for this filter, where the two central cavities are of equal dimensions and the tuning screws are placed in a centered position. Because the filter is symmetrical, only the dimensions of one half of the structure are described. The scattering parameters of this filter are shown in Figure 6, where a frequency response centered at 10 GHz with a 3 dB bandwidth of 600 MHz is shown. The total CPU time for a full-wave analysis considering 401 frequency points was 112 s (notebook Intel i5-580M), thus demonstrating that the implemented CAD tool is indeed very efficient. Moreover, the obtained results are successfully compared with those provided by the commercial simulator Ansys HFSS 13.0, and only small differences are appreciated for the pass-band reflection level.

[34] The next example deals with a five-pole evanescent-mode filter (see topology in Figure 7). In this case, the resonant frequencies are adjusted by means of the height values of the screws, and the separation between the screws is basically used to control the coupling levels. The impedance of the coaxial probe is 50 Ω and it is air filled. This filter is also symmetrical, and all the significative dimensions are included in the caption of Figure 7. The scattering parameters of the designed filter are shown in Figure 8, and a good agreement with HFSS data is observed. The obtained frequency response is also centered at 10 GHz, as the previous designed band-pass filter, but in this case the bandwidth is slightly narrower, with 400 MHz of 3 dB bandwidth. The CPU time for the computation of a complete frequency response with 401 points was 132 s.
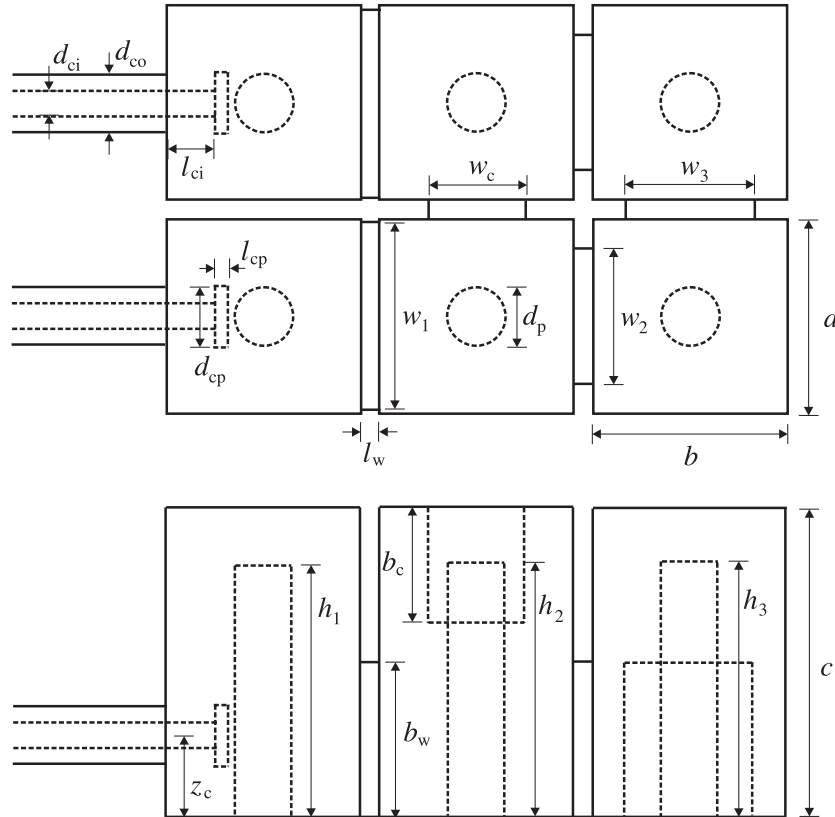
Figure 9. Design of a folded comb-line filter with cross-coupling, whose dimensions (all in millimeters) are: $d_{ci} = 1.3$, $d_{co} = 3.0$, $l_{ci} = 2.5$, $d_{cp} = 3.2$, $l_{cp} = 0.6$, $z_c = 4.21$, $a = b = 10.0$, $c = 16.0$, $l_w = 1.0$, $w_1 = 9.7$, $w_2 = 6.99$, $w_3 = 6.68$, $w_c = 5.0$, $b_w = 8.0$, $b_c = 6.0$, $d_p = 3.0$, $h_1 = 13.015$, $h_2 = 13.163$, $h_3 = 13.22$.

[35] The third example consists of a C-band folded comb-line filter composed of six cavities with a cross-coupling configuration. As it can be seen in Figure 9, the normal coupling between the cavities is magnetic, whereas we obtain an electric coupling by placing the iris on the top of the cavity to introduce a transmission zero. In this case, we have an air-filled coaxial probe and we include a disc-ended coaxial excitation with the aim of increasing the input coupling level. The scattering parameters are shown in Figure 10 for a frequency response centered at 4.75 GHz and a transmission zero placed at the upper side band. In this last example, the CPU time was 197 s for the full-wave analysis of 601 frequency points.

[36] Finally, a C-band folded comb-line filter for satellite applications, considering the presence of tuning screws in the center of the resonant cavities, has been successfully designed, manufactured, and measured. The designed filter and its final dimensions can be found in Figure 11. For validation purposes, a prototype of this designed filter example has been manufactured (see Figure 12). As it can be seen, tuning screws have also been introduced in the coupling windows, for compensating mechanical manufacturing tolerances and fine tuning of the in-band return losses.

[37] In Figure 13, the simulated and measured in-band responses of the comb-line filter are well compared. Apart from compensating the manufacturing tolerances, the tuning screws of the coupling windows have been arranged to enhance the in-band electrical response (return losses) of the real structure. The complete simulation of the originally designed comb-line filter (i.e., without considering the presence of the tuning screws in the coupling windows) has requested a CPU effort of 491 s for the full-wave analysis of 601 frequency points.

Figure 10. Scattering parameters of the folded comb-line filter of Figure 9.
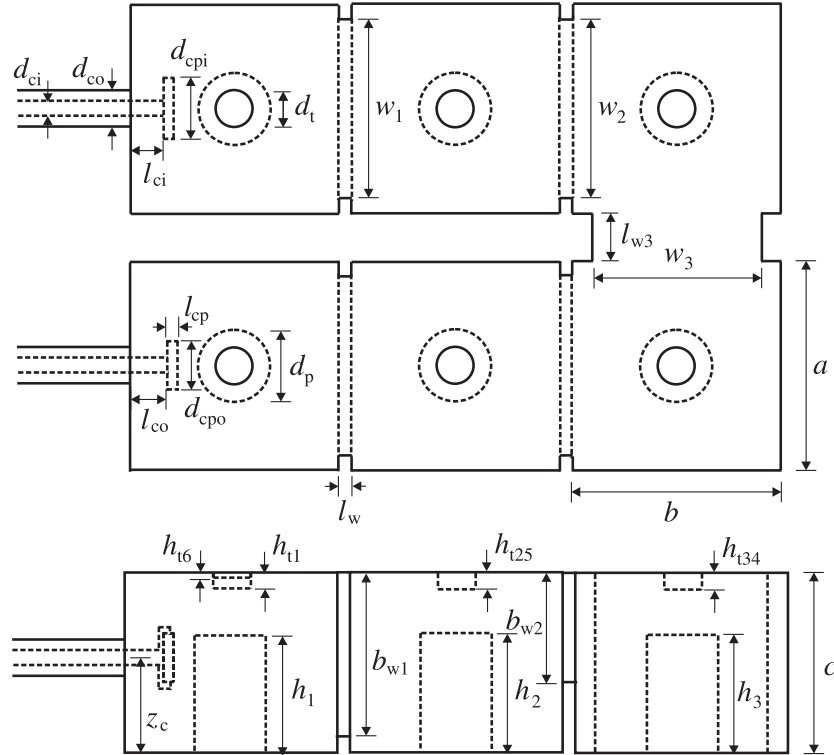
Figure 11. Design of the manufactured folded comb-line filter, whose dimensions (all in millimeters) are: $d_{ci} = 1.27$, $d_{co} = 2.92$, $l_{ci} = 2.81$, $l_{co} = 3.15$ $d_{cpi} = 5.0$, $d_{cpo} = 4.0$, $l_{cp} = 0.8$, $z_c = 8.0$, $a = b = 17.5$, $c = 15.0$, $l_w = 1.0$, $l_{w3} = 4.0$, $w_1 = w_2 = 15.0$, $w_3 = 14.2$, $b_{w1} = 13.69$, $b_{w2} = 9.0$, $d_p = 6.0$, $d_t = 3.15$, $h_1 = 9.98$, $h_2 = 9.93$, $h_3 = 9.81$, $h_{t1} = 1.28$, $h_{t25} = 1.35$, $h_{t34} = 1.355$, $h_{t6} = 0.41$.
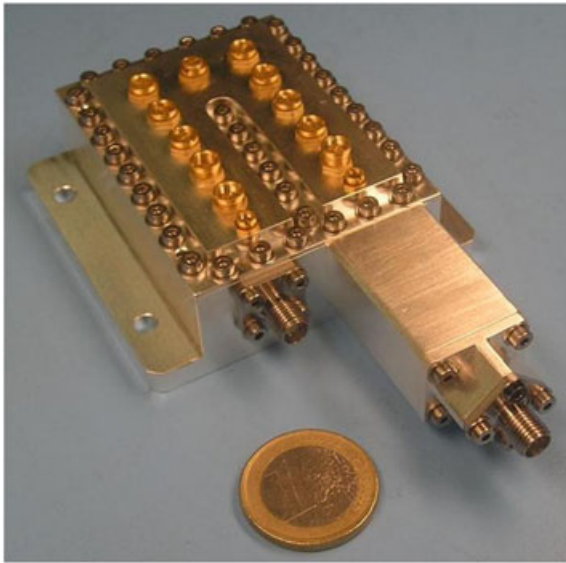
Figure 12. Photograph of the manufactured folded comb-line filter. Courtesy of Thales Alenia Space España.
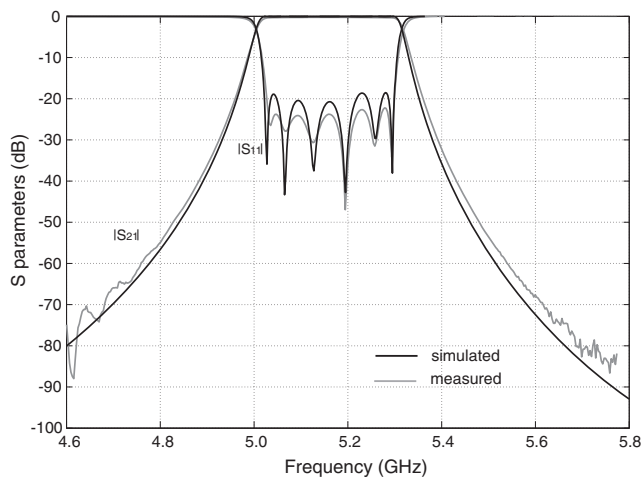
Figure 13. Scattering parameters of the manufactured filter of Figure 12.

5. Conclusion

[38] In this paper, we have presented a very efficient procedure to determine the wideband generalized admittance matrix representation of complex waveguide filters (e.g., in-line direct-coupled-resonator filters with tuning screws, evanescent-mode filters with cylindrical conducting posts, as well as folded configurations of real comb-line filters). These filter structures, widely used in many practical applications, are based on rectangular cavities loaded with partial-height conducting posts, and can also integrate a standard (vertical) or collinear coaxial excitation. The proposed method provides the generalized Y-matrices of the key building blocks in the form of pole expansions, which are then combined through an iterative algorithm providing a global matrix representation of the complete filter structure in the same form. Proceeding in this way, the most expensive computations are performed

outside the frequency loop, thus widely reducing the computational effort required for the analysis of these complex geometries with a high-frequency resolution. The accuracy and numerical efficiency of this new technique have been successfully validated through the full-wave analysis and design of four practical filters implemented in rectangular and coaxial waveguide technologies.

References

Alessandri, F., G. Bartolucci, and R. Sorrentino (1988), Admittance matrix formulation of waveguide discontinuity problems: Computer-aided design of branch guide directional couplers, *IEEE Trans. Microw. Theory Tech.*, *36*(2), 394–403.

Alessandri, F., M. Mongiardo, and R. Sorrentino (1992), Computer-aided design of beam forming networks for modern satellite antennas, *IEEE Trans. Microw. Theory Tech.*, *40*(6), 1117–1127.

Arcioni, P., and G. Conciauro (1999), Combination of generalized admittance matrices in the form of pole expansions, *IEEE Trans. Microw. Theory Tech.*, *47*(10), 1990–1996.

Arcioni, P., M. Bozzi, M. Bressan, G. Conciauro, and L. Perregrini (2002), Frequency/time-domain modeling of 3D waveguide structures by a BI-RME approach, *Int. J. Numer. Model.-Electron. Netw. Device Fields*, *15*(1), 3–21.

Boria, V. E., M. Guglielmi, and P. Arcioni (1998), Computer-aided-design of inductively coupled rectangular waveguide filters including tuning elements, *Int. J. RF Microw. Comput-Aid. Eng.*, *8*, 226–235.

Bozzi, M., L. Perregrini, and K. Wu (2009), A novel technique for the direct determination of multi-mode equivalent circuit models for substrate integrated waveguide discontinuities, *Int. J. RF Microw. Comput-Aid. Eng.*, *19*(4), 423–433.

Bressan, M., L. Perregrini, and E. Regini (2000), BI-RME modeling of 3D waveguide components enhanced by the Ewald technique, *IEEE MTT-S Int. Microw. Symp. Dig.*, *2*, 1097–1100.

Chang, H. C., and K. A. Zaki (1991), Evanescent-mode coupling of dual-mode rectangular waveguide filters, *IEEE Trans. Microw. Theory Tech.*, *39*(8), 1307–1312.

Gentili, G. G. (2001), Multiport analysis of arbitrary circular-rod insets in rectangular waveguide by the generalized admittance matrix, *IEEE Trans. Microw. Theory Tech.*, *49*(8), 1438–1442.

Gerini, G., M. Guglielmi, and G. Lastoria (1998), Efficient integral equation formulations for admittance or impedance representation of planar waveguide junctions, *IEEE MTT-S Int. Microw. Symp. Dig.*, *3*, 1747–1750.

Gimeno, B., and M. Guglielmi (1997), Multimode equivalent network representation for junctions between coaxial and circular waveguides, *Int. J. Microw. Millimet. Wave Comput-Aid. Eng.*, *7*(2), 180–194.

Guglielmi, M. (1994), Simple CAD procedure for microwave filters and multiplexers, *IEEE Trans. Microw. Theory Tech.*, *42*(7), 1347–1352.

Höft, M., and F. Yousif (2011), Orthogonal coaxial cavity filters with distributed cross-coupling, *IEEE Microw. Wirel. Compon. Lett.*, *21*(10), 519–521.

Ihmels, R., and F. Arndt (1993), Field theory CAD of L-shaped iris coupled mode launchers and dual-mode filters, *IEEE MTT-S Int. Microw. Symp. Dig.*, 765–768.

Levy, R., H. W. Yao, and K. A. Zaki (1997), Transitional combline/evanescent mode microwave filters, *IEEE Trans. Microw. Theory Tech.*, *45*(12), 2094–2099.

Liang, J., H. Chang, and K. A. Zaki (1992), Coaxial probe modeling in waveguides and cavities, *IEEE Trans. Microw. Theory Tech.*, *40*(12), 2172–2180.

Mansour, R. R., and R. H. MacPhie (1986), An improved transmission matrix formulation of cascaded discontinuities and its application to E-plane circuits, *IEEE Trans. Microw. Theory Tech.*, *34*(12), 1490–1498.

Marcuvitz, N. (1986), *Waveguide Handbook*, Peter Peregrinus, London.

Mira, F., M. Bressan, G. Conciauro, B. Gimeno, and V. E. Boria (2005a), Fast S-domain method of rectangular waveguides with radially-symmetric metal insets, *IEEE Trans. Microw. Theory Tech.*, *53*(4), 1294–1303.

Mira, F., A. A. San Blas, V. E. Boria, B. Gimeno, and G. Conciauro (2005b), Fast and accurate CAD tool of passive rectangular waveguide devices including cylindrical conducting posts, *Proc. 35th Eur. Microw. Conf.*, 939–942.

Mira, F., A. A. San Blas, V. E. Boria, and B. Gimeno (2008), Efficient pole expansion of the generalized admittance matrix representation of planar waveguide junctions, *Proc. 38th Eur. Microw. Conf.*, 650–653.

Mira, F., A. A. San Blas, V. E. Boria, and B. Gimeno (2009), Wideband impedance matrix representation of passive waveguide components based on cascaded planar junctions, *Radio Sci.*, *44*, *RS1004, doi*:10.1029/2008RS003886.

Morini, A., G. Venanzoni, and T. Rozzi (2006), A new adaptive prototype for the design of side-coupled coaxial filters with close correspondence to the physical structure, *IEEE Trans. Microw. Theory Tech.*, *54*(3), 1146–1153.

Morini, A., G. Venanzoni, M. Farina, and T. Rozzi (2007), Modified adaptive prototype inclusive of the external couplings for the design of coaxial filters, *IEEE Trans. Microw. Theory Tech.*, *55*(9), 1905–1911.

Quesada, F. D., A. Vidal, F. J. Pérez, A. Berenguer, A. A. San Blas, F. Mira, V. E. Boria, B. Gimeno and A. Álvarez (2010), Broad band analysis of arbitrarily shaped microwave filters using a novel singular value decomposition technique, *Proc. 4th Eur Conf. Ant. Prop. (EuCAP)*, 1–3.

San Blas, A. A., F. Mira, V. E. Boria, B. Gimeno, G. Conciauro, M. Bressan, and P. Arcioni (2006), Efficient CAD of generalized coaxial probes in rectangular waveguide using the 3D BI-RME method, *Proc. 36th Eur. Microw. Conf.*, 1163–1166.

Uher, J., J. Bornemann, and U. Rosenberg (1993), *Waveguide Components for Antenna Feed Systems: Theory and CAD*, Artech House, Norwood.

Yao, H. W., K. A. Zaki, A. E. Atia, and R. Hershtig (1995), Full wave modeling of conducting posts in rectangular waveguides and its application to slot coupled combline filters, *IEEE Trans. Microw. Theory Tech.*, *43*(12), 2824–2830.